Wanisa Salaemae, Min Y. Yap, Kate L. Wegener, Grant W. Booker, Matthew C.J. Wilce, Steven W. Polyak

Nucleotide triphosphate promiscuity in Mycobacterium tuberculosis dethiobiotin synthetase

Tuberculosis, 2015; 95(3):259-266

Nucleotide Triphosphate Promiscuity in *Mycobacterium tuberculosis* Dethiobiotin Synthetase

Wanisa Salaemae[a], Min Y. Yap [b#], Kate L. Wegener[a], Grant W. Booker[a], Matthew C.J. Wilce[b], and Steven W. Polyak[a*]

[a]School of Biological Sciences, The University of Adelaide, South Australia, Australia 5005

[b]Department of Biochemistry and Molecular Biology, School of Biomedical Science, Monash University, Victoria, Australia 3800

Running title: *Promiscuous NTP binding to mycobacterial Dethiobiotin synthetase*

*Corresponding author: Department of Molecular and Cellular Biology, School of Biological Sciences, The University of Adelaide, South Australia, Australia 5005, Tel.: +61 8 8313 6042; E-mail: steven.polyak@adelaide.edu.au

[#]Current address: CSL Limited, 45 Poplar Road, Parkville, Victoria 3052, Australia

Abbreviations:

DAPA, (7R, 8S)-7,8-diaminopelargonic acid; DTB, dethiobiotin; DTBS, dethiobiotin synthetase; IMAC, immobilized metal affinity chromatography; SEC-MALS, size exclusion multi angle light scattering; SPR, surface plasmon resonance

SUMMARY

Dethiobiotin synthetase (DTBS) plays a crucial role in biotin biosynthesis in microorganisms, fungi, and plants. Due to its importance in bacterial pathogenesis, and the absence of a human homologue, DTBS is a promising target for the development of new antibacterials desperately needed to combat antibiotic resistance. Here we report the first X-ray structure of DTBS from *Mycobacterium tuberculosis* (*Mt*DTBS) bound to a nucleotide triphosphate (CTP). The nucleoside base is stabilized in its pocket through hydrogen-bonding interactions with the protein backbone, rather than amino acid side chains. This resulted in the unexpected finding that *Mt*DTBS could utilise ATP, CTP, GTP, ITP, TTP, or UTP with similar K_m and k_{cat} values, although the enzyme had the highest affinity for CTP in competitive binding and surface plasmon resonance assays. This is in contrast to other DTBS homologues that preferentially bind ATP primarily through hydrogen-bonds between the purine base and the carboxamide side chain of a key asparagine. Mutational analysis performed alongside *in silico* experiments revealed a gate-keeper role for Asn175 in *Escherichia coli* DTBS that excludes binding of other nucleotide triphosphates. Here we provide evidence to show that *Mt*DTBS has a broad nucleotide specificity due to the absence of the gate-keeper residue.

Keywords: enzyme, biotin biosynthesis; dethiobiotin synthetase; nucleotide triphosphate; crystal structure, *Mycobacterium tuberculosis*; *Escherichia coli*.

1. INTRODUCTION

De novo synthesis of biotin (aka vitamin H or B7) is an important metabolic activity for microorganisms, fungi and plants, which is not present in humans [1]. In bacteria, biotin serves as an essential cofactor for biotin-dependent enzymes, namely pyruvate carboxylase (PC) to replenish the Krebs cycle and acyl-CoA carboxylase (ACC) for membrane biogenesis and maintenance [2], [3], [4] and [5]. As the cell membrane provides a defensive barrier against environmental toxins, host immune factors and antibiotic agents [6] and [7], the metabolic pathways related to the synthesis of membrane lipids have been suggested as promising targets for the development of new antibiotics. Genetic studies have revealed important roles for biotin biosynthesis in *Mycobacterium tuberculosis* during growth, infection and the latency phase, thus establishing this pathway as a potential drug target for new anti-tuberculosis therapies [3], [8], [9], [10], [11] and [12]. In addition, biotin biosynthesis has been intensively studied in other bacteria and the enzymes involved in the pathway have been implicated in bacterial virulence during infection and intracellular replication [13].

Dethiobiotin synthetase (DTBS, EC 6.3.3.3, encoded by *bioD*) controls the penultimate step of the biotin biosynthesis pathway, catalysing the closure of the ureido ring of dethiobiotin (DTB) from (7R, 8S)-7,8-diaminopelargonic acid (DAPA) using CO_2 and a nucleotide triphosphate (NTP). The reaction mechanism has been proposed to involve three discrete steps, which are (1) the formation of N7-carbamate, (2) the formation of the carbamic-phosphoric acid anhydride, and (3) the closure of the ureido ring with the release of inorganic phosphate [14]. The amino acid residues required for binding the DAPA substrate and subsequent catalysis have been well characterized, with X-ray crystal structures available for the enzymes from *Escherichia coli, M. tuberculosis, Helicobacter pylori*, and *Francisella tularensis* [15], [16], [17] and [18]. However, the molecular details of NTP binding are less well defined, especially for *M. tuberculosis* DTBS (*Mt*DTBS) where there is currently no crystal structure of the enzyme in complex with NTP. From the available structural data, the NTP binding site is divided into two discrete subsites; the phosphate-binding region (also known as the P-loop or Walker A

motif) and the nucleoside-binding pocket. In *E. coli* DTBS (*Ec*DTBS), a conformational change involving the P-loop (Gly8-X-X-X-X-Gly14-Lys15-Th16) was observed following phosphate binding [16]. In contrast, a comparison of available *Mt*DTBS structures revealed no homologous conformational change upon the binding of inorganic phosphate [15]. Comparison of the bacterial DTBS homologues revealed considerable structural differences in nucleoside recognition at the C-terminal region of DTBS [18]. For example, Asn175 in *Ec*DTBS, found within the [**N**Q]-[KR]-x-[DE] GTP specificity motif, has been proposed to play a key role in the adenosine specificity observed for *E. coli*, *H. pylori* and *F. tularensis*. However this amino acid is absent in *Mt*DTBS, which instead contains a glycine at the equivalent position (G169). As nucleotide analogs have proved a successful route to new drugs, there is the potential to likewise target the nucleotide pocket of DTBS for new antibiotics. Narrow spectrum therapeutics with anti-tuberculi activity would be especially welcome in the fight against tuberculosis. However, this requires a greater understanding of the nucleotide binding pockets of bacterial DTBS enzymes and the molecular basis of NTP binding.

Previous attempts to characterize DTBS have been restricted by the lack of facile assays. DTBS activity was commonly measured with a spectrophotometric assay by monitoring ADP production through the coupling of pyruvate kinase and lactate dehydrogenase [19], [16], [19] and [16]. Using two additional enzymes in the reaction is less than desirable for high-throughput screening applications. An alternative radioactive-labeled carbon fixation assay has been reported for detecting the formation of the acid-stable [^{14}C]DTB product using [^{14}C]CO_2 [19]. However, complicated procedures are required to remove excess [^{14}C]CO_2 from the reaction. Recently, a continuous fluorescent assay was developed to detect the coupled action of DAPAS and DTBS, based on the displacement of a dethiobiotin fluorescent probe bound to streptavidin by the DTB product [20]. Although, it is possible to adapt this continuous fluorescent assay for detecting the DTBS activity alone, the fluorescent probe is not commercially available and must be synthesized via at least four steps [21] and [20].

In this study, we successfully developed two facile, homogeneous assays to study DTBS. These enabling technologies will be beneficial for future drug discovery efforts.

Here the assays were employed to characterize DTBS from *E. coli* and *M. tuberculosis*. The specificity of NTP binding and utilization was investigated. Stark differences were observed between the two enzymes with *Ec*DTBS having highest preference for ATP whereas *Mt*DTBS showed equal potency for a broad panel of NTPs. A competitive ATP binding assay together with surface plasmon resonance analysis (SPR) showed that CTP bound to the mycobacterium homologue with greatest affinity. For the first time, the structure of *Mt*DTBS was resolved in complex with a nucleotide, namely CTP. X-ray crystallography in combination with mutagenesis studies revealed a role for N175 in *Ec*DTBS in discriminatory binding of NTPs.

2. MATERIALS AND METHODS

2.1 *Cloning and plasmid construction.*

The *bioD* genes encoding DTBS from *M. tuberculosis* strain H37Rv (Gene ID: 886338) and *E. coli* strain K-12 (Gene ID: 945387), both containing an N-terminal hexa-histidine tag, were synthesized as codon optimized genes for expression in *E. coli* and ligated into the pMA vector (GENEART® Gene Synthesis, Life Technologies Australia Pty Ltd.). Site directed mutagenesis was performed using the QuickChange® site-directed PCR mutagenesis kit (Stratagene) with oligonucleotides synthesized at GeneWorks Pty Ltd (Adelaide, Australia). All oligonucleotides used in this study are listed in Table S1. The *Mt*DTBS-G169N mutation was constructed using oligonucleotides A1 and A2 whereas the two mutants of *Ec*DTBS were constructed with oligonucleotides A3 and A4 for *Ec*DTBS-N175G and A5 and A6 for *Ec*DTBS-N175A. For recombinant expression in *E. coli*, the coding regions were subcloned into *Nco*I and *Hind*III treated pET16b vector (Novagen). All constructs were verified by DNA sequencing using the Gene Sequencing Service, SA Pathology (Adelaide, Australia).

2.2 Expression and Protein Purification

DTBS proteins were recombinantly expressed in *E. coli* strain BL21(DE3) (Invitrogen). Cultured cells were used to inoculate LB medium containing 0.1 mg ml^{-1} ampicillin and grown at 37 ˚C until early log phase when protein expression was induced with 0.1 mM IPTG. For *Ec*DTBS and its mutants the cell cultures were induced at 37 ˚C for 3 h, whereas the *Mt*DTBS and its mutant were grown for 18 hours at 25 ^{o}C. Cells were harvested by centrifugation at 4648 x *g* for 15 min and resuspended in 300 mM KCl, 50 mM potassium phosphate buffer (pH 8.0), 5 mM imidazole and 1 mM PMSF. Cells were lysed using a Microfluidics Cell Disruptor at 18 000 psi and debris removed by centrifugation at 48 384 x *g* for 30 min. His-tagged DTBS proteins were purified by

immobilized metal affinity chromatography (IMAC) using the Profinia® IMAC protocol following the manufacturer's instructions (BIO-RAD). After elution in 50 mM potassium phosphate buffer (pH 8.0), 300 mM KCl and 250 mM imidazole, the proteins were subsequently buffer exchanged into storage buffer (25 mM Tris buffer (pH 7.5), 30 mM NaCl, 1 mM EDTA, 1 mM dithiothreitol and 5% (v/v) glycerol) using a 50 ml Bio-Scale™ Mini Bio-Gel® P-6 desalting cartridge (BIO-RAD). For insoluble *Mt*DTBS-G169N the inclusion bodies were solubilized in 8 M Urea (pH 8.0), 100 mM Tris, 300 mM NaCl and 5 mM imidazole. The urea buffer was first deionized using the Mixed Bed Resin (Sigma Aldrich®) following the manufacturer's protocol. The solubilized sample was centrifuged at 48 384 x *g* for 30 min, before fractionation using the Profinia® Denaturing IMAC protocol following the manufacturers' instructions (BIO-RAD). *Mt*DTBS-G169N was eluted in 8 M Urea (pH 8.0), 100 mM Tris, 300 mM NaCl and 250 mM imidazole, then diluted to 0.2 mg ml^{-1} for refolding. The protein was dialyzed extensively against storage buffer for 48 hours by changing the buffer four times (1:100 (v/v)). DTBS proteins were concentrated using Amicon Ultra-15 centrifugal filter devices (Millipore), followed by centrifugation at 15 700 x *g* for 15 min to discard protein aggregates. Protein concentrations were determined using a Bradford Protein Assay (BioRad) using bovine serum albumin (Sigma Aldrich®) as a standard.

2.3 *Protein Methods*

Estimation of the molecular weight of active DTBS material was performed by size exclusion chromatography – multi-angle light scattering (SEC-MALS) analysis. The instrument consisted of a Superdex 200 10/300 GL column (Amersham Biosciences) connected in series with a miniDAWN TREOS light-scattering detector (Wyatt Technology) and an OPTILAB rEX interferometric refractometer detector (Wyatt Technology). Analytical size-exclusion chromatography was performed at 20° C using a mobile phase containing 25 mM Tris pH 7.5, 30 mM NaCl and 1 mM EDTA at a flow rate of 0.25 mL/min. Detector outputs were acquired using Astra software (Wyatt Technology).

The identities of the purified wildtype proteins were confirmed by enzyme assay and liquid chromatography-electrospray ionization tandem mass spectrometry, whilst the molecular weight of the mutants were confirmed using MALDI mass spectrometry, as described in Supporting Methods. All mass spectrometry services were performed at the Adelaide Proteomics Center, The University of Adelaide.

2.4 *Preparation of Nucleotide triphosphates*

Solutions of NTPs were prepared by dissolving solid compound in sterile water and adjusting the pH to 7.0 with sodium hydroxide. The final concentration was determined by measuring absorbance at 260 nm, as described in [22]. For assays, the NTPs were first mixed with an equimolar concentration of $MgCl_2$ solution to form a MgNTP complex.

2.5 *DTBS Enzyme Assay*

The activity of DTBS was determined using fluorescence-polarization (FP) technology to quantify the amount of synthesized DTB that could displace fluorescein-biotin (Anaspec Inc) from streptavidin. All experiments were performed in black 96 well microtiter plates (Costar®) preblocked with 1% casein dissolved in Tris-buffered saline. Assays were performed at 37 ˚C in FP buffer (50 mM Tris (pH 7.5), 150 mM NaCl, 5 mM $MgCl_2$, and 10 mM $NaHCO_3$ (or 50 mM $NaHCO_3$ for *Mt*DTBS-G169N) supplemented with 0.3 mM ATP and 0.1 mM DAPA (Toronto Research Chemicals, Inc.). Assays were initiated with the addition of DTBS enzyme. The concentration of DTBS in the reaction (at 0.25 – 3.0 μM) varied depending on its species of origin or mutant employed. The reactions were terminated within the initial, linear phase of the reaction at 45 min by the addition of 50 mM Tris (pH 7.5), 150 mM NaCl, and 250 mM EDTA and then incubated for 15 min at 37 ˚C. The synthesized DTB product was detected by adding 20 nM streptavidin in 50 mM Tris (pH 7.5), 150 mM NaCl and incubating for 15 min at 37 °C before the addition of 25 nM fluorescein biotin in 50 mM Tris (pH 7.5), 150 mM NaCl. Finally, the reaction mixtures were incubated at 37˚C for 15 min before FP was measured with a

PerkinElmer 2030 Plate Reader using polarization mode set to 485 nm excitation and 535 nm emission [23]. FP is defined as the difference of the emission light intensity parallel and perpendicular to the excitation light plane; normalized by the total fluorescence emission intensity [24] and [25]. The concentration of enzymatically generated DTB was calculated from a standard curve generated with each experiment (see example in Fig. S6) and using Equation 1; a linear regression binding model where S is the slope of the standard curve, Y is the Y intercept and delta mP is the corrected FP value (ie mP (streptavidin) – mP (no streptavidin control)).

$$\text{Log (DTB (M))} = -(\text{delta mP} + Y)/S \qquad \text{(Eq. 1)}$$

The data were fit to the Michaelis–Menten equation and the V_{max} and K_m were then calculated using GraphPad Prism 6 (GraphPad Software, Inc.).

2.6 *DTBS ATP-binding Assay*

The binding of a fluorescently-labeled ATP tracer, ATP-BODiPY (Life Technologies^{TM}), to DTBS was performed in binding buffer containing 0.1 mM DTBS, 50 mM Tris (pH 7.5), 150 mM NaCl, and 5 mM $MgCl_2$. Varying concentrations of MgNTPs were included and the reaction pre-equilibrated for 15 min before the addition of 25 nM ATP-BODiPY. The reaction was performed at 37 ˚C for 15 min and fluorescence polarization measured as described above. The IC_{50} was measured by plotting the corrected FP values (delta mP = mP(DTBS) – mP (no DTBS control)) against log of MgNTP concentration and fitting the data to a log (inhibitor) versus response – variable slope (four parameters) model in GraphPad Prism 6 (GraphPad Software, Inc.).

2.7 *Surface Plasmon Resonance (SPR)*

The kinetics of the interaction between DTBS and NTP were analyzed using a BIAcore T100. Details of the protein immobilization and data analysis are described in the Supporting Information. Flow cell 1 of the sensor chip was used as reference to correct

for bulk refractive index changes. Immobilized bovine serum albumin was also employed as control for non-specific binding. Varying concentrations of MgNTP were prepared in running buffer (10 mM HEPES (pH 7.4), 150 mM NaCl and 0.005% (v/v) surfactant P20) then injected across the sensor surface. The equilibrium binding constant (K_D) was determined using an affinity-steady state 1:1 model in BIAcore T100 evaluation software (GE Healthcare).

2.8 *X-ray Crystallography*

*Mt*DTBS was concentrated to 10 mg ml^{-1}, to which a final concentration of 1 mM CTP was added and incubated for 1 hour at room temperature. The complex was crystallized using the hanging drop vapour diffusion method at room temperature. Crystals grew from the following range of buffers: 0.8 - 1.2 M ammonium sulphate, 0.1 M Tris pH 7 - 8.5 with 10 % glycerol. X-ray diffraction data was collected in-house using a Rigaku RUH2R rotating copper anode X-ray source equipped with Osmic confocal optics and an R-Axis IV detector. Crystals were flash frozen and the diffraction data collected with cryo-cooling using an Oxford Cryosystems 700 Series cryostream at 100 K. The diffraction data was indexed, merged and integrated using XDS [26], which was also used to produce the final MTZ files required for structure refinement. Initial phases of the structure were determined with PHASER [27] using the co-ordinates of *Mt*DTBS (PDB ID: 3FGN) as a search model. The model of *Mt*DTBS in complex with CTP was built with cycles of manual modeling with COOT [28] and refinement with PHENIX [29]. The co-ordinates were deposited in the protein database 4WOP.

3. RESULTS

3.1 *Purification and biochemical characterization of M. tuberculosis and E. coli DTBS.*

Genes encoding the two bacterial DTBS enzymes were synthesized and cloned into the pET-16b plasmid for recombinant expression in *E. coli*. A hexa-histidine tag was engineered onto the N-terminus of the proteins to facilitate purification using immobilized nickel affinity chromatography. *Ec*DTBS expressed as a soluble protein at 37˚C, whereas the optimal conditions for the *M. tuberculosis* equivalent were overnight at 25˚C. SDS-PAGE analysis of the IMAC purified material revealed high purity (>95%) and a single product corresponding to the expected molecular mass of 23.5 kDa for *Mt*DTBS or 25.1 kDa for *Ec*DTBS (Fig. S1). Liquid chromatography-electrospray ionization tandem mass spectrometry analysis of the tryptic peptides confirmed the identity of the purified material, with 47% coverage for *Mt*DTBS and 41% coverage for *Ec*DTBS (Table S2). SEC-MALS analysis revealed that >98% of the total proteins eluted at a molecular mass consistent with a homodimer (Fig. S2A&B). Interestingly, MS/MS sequencing failed to detect endogenous *E. coli* protein in the *Mt*DTBS preparation implying the recombinant mycobacterial protein did not form heterodimers with the host protein.

3.2 *Enzyme Activity and Assay Development*

To characterize the purified enzymes two alternative assays were developed to measure enzyme activity and ATP binding. Both assays incorporated fluorescence polarization technology to quantify the difference in anisotropy of a fluorescent tracer between its free and protein-bound states [30], [31] and [32]. The enzyme assay exploits the observation that DTB, enzymatically produced by DTBS, effectively competes with commercially available fluorescein-biotin (M_r 831 Da) to bind streptavidin (M_r 67 000 Da). Notably, the tracer did not bind to DTBS (Fig. S3A). Furthermore DTB, but not the substrate DAPA, could displace the tracer from streptavidin (Fig. S3B). The

ATP binding-assay exploits the large mass difference observed between free ATP-BODiPY (M_r 933 Da) and the tracer in complex with DTBS (Mr 23 500 Da for *Mt*DTBS; 25 100 Da for *Ec*DTBS). The binding of ATP tracer to DTBS was found to be independent of DAPA substrate (Fig. S3C). Both approaches provide convenient, homogenous assays using commercially available reagents that yield complementary data to quantify the mechanism of ligand binding. The apparent K_M for DAPA, $NaHCO_3$ and ATP were obtained using steady-state kinetic analysis, varying the concentration of one substrate whilst maintaining the two others at saturating concentrations. The K_M values for DAPA and $NaHCO_3$ were calculated to be 15.2 ± 1.7 μM and 0.6 ± 0.1 mM for *Ec*DTBS and 30.2 ± 1.1 μM and 3.1 ± 0.4 mM for *Mt*DTBS, respectively (Table 1). In this study, the K_M for ATP for *Mt*DTBS (30.2 ± 1.7 μM) was 3-fold higher than that of *Ec*DTBS (10.5 ± 0.8 μM), but these values were in excellent agreement with published literature for the two enzymes [15, 33].

The activity of the DTBS enzymes was initially measured in the presence of each of a panel of NTPs at 0.3 mM. Unexpectedly, *Mt*DTBS was able to utilize any of ATP, CTP, GTP, ITP, TTP and UTP (Fig. 1). These observations were in stark contrast to the *E. coli* homologue where the enzyme had greatest preference for ATP, a result consistent with published literature [33]. Further kinetic analysis showed that *Mt*DTBS utilized all nucleotides with similar K_M's and k_{cat}'s while *Ec*DTBS could use CTP and GTP albeit with more than 100-fold and 150-fold higher K_Ms than ATP, respectively (Fig. 2 & Table 1). This nucleotide specificity was confirmed in the ATP-binding assay where all nucleotides could compete effectively against the ATP-BODiPY tracer for binding *Mt*DTBS (Fig. 3). Here, CTP was observed to have the greatest binding affinity with a 6-fold lower IC_{50} than ATP in *Mt*DTBS (Table 2). Consistent with the enzyme assay, ATP was the preferred NTP in *Ec*DTBS with >10-fold lower IC_{50} values than CTP and GTP. SPR analysis was also employed to measure the bimolecular interactions between DTBS and nucleotide triphosphates. Again, this confirmed that both ATP and CTP bound to *Mt*DTBS (Fig. 4A) with CTP demonstrating the highest affinity (K_D CTP = 17.2 ± 1.7 μM; ATP = 335.1 ± 96.0 μM) (Fig. S4A&B). In contrast, *Ec*DTBS was highly selective for ATP (K_D of 347.9 ± 75.1 μM) over CTP where no response was observed (Fig. 4B and Fig. S4C). Injection of NTPs over either an empty flow cell or immobilized

bovine serum albumin (BSA), performed concurrently with the immobilized DTBS experiment, resulted in negligible response (Fig 4D, and data not shown). This confirmed the specificity of NTP binding to the DTBS enzymes.

3.3 *X-ray Crystallography* – To date there have been no X-ray structures available of *Mt*DTBS in complex with a nucleotide triphosphate. To better understand the molecular basis of ligand binding, *Mt*DTBS was crystallized in complex with CTP (Fig. 5). The structure was determined to 2.3 Å; data collection, refinement, and geometric statistics are provided in Table S3. Repeated attempts to crystallize the enzyme with ATP were unsuccessful. As expected, our structures were consistent with the α/β-fold observed in the published structures for *E. coli*, *H. pylori* and *F. tularensis* DTBS [18]. Superimposition of chain D of our structure against chain D of a previously reported apo-structure for *M. tuberculosis* (PDB # 3FGN [15]) had the lowest RMSD of 0.387 Å (for 224 Cα atoms), and the same fold of a seven-stranded parallel β-sheet surrounded by seven helices. Superimposition of the two dimeric forms of the crystallized structures (chain A and B) were also in excellent agreement with an RMSD of 0.40 Å (for 225 Cα atoms). These results indicated that there are no large conformational changes that accompany CTP binding. Whilst the enzyme crystallized as a dimer of dimers, the NTP-binding site is distant from the dimer interface and all the residues contacting the NTP are present within a single subunit. *Mt*DTBS possesses the classical P-loop motif (Walker A motif) with Gly12, Val13, Gly14, Lys15 and Thr16 all forming hydrogen bonding interactions with the triphosphate moiety on CTP. A series of hydrophobic interactions involving C2 and the 2' hydroxyl on the ribose with the side chain of Val 17 and the beta carbon of Ala 201 stabilize the sugar in its binding pocket (Fig. S5). CTP adopted a bent conformation with rotation around the C-N bond between ribosyl and cytosinyl groups to allow the pyrimidine ring to bind in its appropriate pocket. Two hydrophobic interactions are observed between the pyrimidine ring and the protein, namely C5 with Ser170 and C6 with Val17 in the P-loop. The interaction is further stabilized through three hydrogen-bonding interactions with the pyrimidine ring. What is noteworthy is that all three of these bonds are with the protein backbone and not with

amino acid side chains; O2 bonds with the nitrogen of Ala201 whilst N4 bonds with the backbone oxygen atoms of Gly169 and Pro197.

The lack of side chain interactions contacting the nucleotide base observed in *Mt*DTBS is in contrast to the *E. coli* homologue, in which the carboxamide side chain on Asn175 forms hydrogen-bonding interactions with N6 and N7 on the purine ring of ATP (Fig. 6) [14]. This side chain interaction is also present in *H. pylori*, which selectively binds ATP [18]. It has previously been proposed that side chain interactions involving asparagine play a key role in nucleotide specificity [34] and [18], but this has not been tested experimentally. To uncover the function of this asparagine in NTP binding, an asparagine residue was engineered into the *M. tuberculosis* enzyme at the structurally equivalent position to Asn175 in *Ec*DTBS, thereby generating *Mt*DTBS-G169N. Likewise, two muteins of the *E. coli* homologue were generated by substituting Asn175 with either glycine or alanine (producing *Ec*DTBS-N175G and *Ec*DTBS-N175A).

3.4 Purification and biochemical characterization of mutants

*Ec*DTBS-N175G and *Ec*DTBS-N175A were expressed as soluble proteins in *E. coli* allowing their purification by IMAC. In contrast, *Mt*DTBS-G169N formed inclusion bodies and, therefore, required refolding. *Mt*DTBS-G169N was purified using IMAC under denaturing conditions and then refolded by a four step-wise dialysis procedure to restore enzyme activity. SEC-MALS analysis revealed that only 25% of the refolded *Mt*DTBS-G169N material eluted as a homodimer, with the majority of the material forming inactive protein aggregates (Fig. S2C). Following size exclusion chromatography the specific enzyme activity of active, dimeric *Mt*DTBS-G169N (56.2 μM min^{-1} mg^{-1}) was comparable to that measured for the wildtype *Mt*DTBS (74.0 μM min^{-1} mg^{-1}). To confirm the identity of the muteins, MALDI mass spectrometry was performed. The measured molecular mass corresponding to methionine removed DTBS $[M+H]^+$ was in agreement with the predicted molecular mass (Table S4).

The mutant enzymes all showed K_M values for DAPA comparable to their wildtype counterparts (Table 1), suggesting that the introduced mutations had not compromised

enzymatic activity nor the DAPA binding site. Whilst the two substitutions in the *E. coli* enzyme had no significant effect on the K_M for $NaHCO_3$, the G169N mutation in *Mt*DTBS elevated the K_m for the carbonate 3-fold (WT *vs* G169N, $p<0.05$) (Table 1). The molecular explanation for this is unclear.

Substitution of N175 in *Ec*DTBS with alanine or glycine had no effect on the K_M for ATP (*Ec*DTBS-N175G *vs* WT, p=0.11; *Ec*DTBS-N175A *vs* WT p=0.19). Whilst the K_m for CTP was not significantly different for *Ec*DTBS-N175G, the introduction of alanine significantly lowered the K_M for CTP by 2.7-fold (*Ec*DTBS-N175A *vs* WT, $p<0.05$) implying that hydrophobic interactions help stabilize the interaction between protein and NTP. This was supported by SPR analysis that also demonstrated that the binding of CTP was improved for *Ec*DTBS-N175A (Fig. 4C). These kinetic data are in contrast to the *Mt*DTBS-G169N mutant. Whilst the affinity for ATP was again unchanged (*Mt*DTBS-G169N *vs* WT, $p = 0.09$), the asparagine substitution significantly elevated the K_M for both CTP and GTP by 1.8-fold and 3.8-fold respectively. Unfortunately, attempts to immobilize the *Mt*DTBS-G169N for SPR analysis were unsuccessful. Together these data support a role for N175 in excluding other NTPs from the nucleoside-binding pocket, thus allowing selective binding of ATP. Without the ‘gate keeper’ asparagine, *Mt*DTBS can accommodate a broad range of NTPs.

4. DISCUSSION

It has previously been proposed that DTBS is more similar to GTP-binding proteins than ATP-dependent enzymes based on its fold [35] and the presence of the [NQ]-[KR]-x-[DE] GTP specificity motif in the *E. coli*, *H. pylori* and *F. tularensis* enzymes (containing NDVTP, NLKGN, and NCNDS motifs respectively) [18]. The first asparagine in this motif (numbering N175 in *Ec*DTBS) was suggested to be an evolutionary relic from a protein able to bind both adenosine and guanine nucleotides and provides nucleotide specificity [34] and [18]. Curiously, in the current study, DTBS from *M. tuberculosis* was shown to be capable of binding ATP and GTP, as well as other nucleotides, with similar affinities despite the enzyme being devoid of the equivalent asparagine. Here, for the first time, we present the structure of *Mt*DTBS in complex with a nucleotide (CTP). The structural data revealed that the hydrogen bonding interactions with the nucleoside occurred exclusively through the peptide backbone of the enzyme, and not via side chains. Indeed, with the absence of Asn175 (equivalent position of G169 in *Mt*DTBS) or the reduction of hydrophobic interactions at C5 of the pyrimidine ring with S170 (*Mt*DTBS-S170D, data not shown), the *Mt*DTBS retained the ability to bind all nucleotides.

To further understand the molecular basis of NTP binding to DTBS, we superimposed the structure of *Ec*DTBS in complex with ATP (PDB # 1A82 [14]) and *Hp*DTBS in complex with ATP or GDP (PDB # 3QXC, 3QXX [18]) onto the CTP bound *Mt*DTBS structure. In the published X-ray structures, ATP and GTP both adopt an extended conformation that would cause a significant steric clash with *Mt*DTBS in the nucleotide-binding pocket. Compared to the more open pockets observed in *Ec*DTBS and *Hp*DTBS, *Mt*DTBS has a more constrained pocket due to additional strands at the C-terminus of the enzyme. Presumed flexibility at the loops formed by G169 – W171 and A195 – A201 would allow accommodation of other NTPs in the nucleotide pocket.

The biological significance of the selective binding reported here may be a function of the concentrations of NTPs found in different bacteria. For *E. coli* and *Salmonella enterica*, it has been reported that ATP is the most abundant NTP, with concentrations

being at least 3 mM [36] and [37]. This is >300 times above the K_M for ATP measured in this study for *Ec*DTBS suggesting that ATP is constantly at saturating concentrations *in vivo*. The levels of various NTPs can decrease as *E. coli* transitions from growth to stationary phase. Interestingly, of all the NTPs, CTP had the most constant concentration throughout the whole growth curve, with only minor fluctuations in its levels. *In Mycobacteria* there is an abundant supply of all NTPs during all stages of cell growth [38]. Here nucleoside diphosphate kinase plays an important role in NTP synthesis by utilizing both purine and pyrimidine NDP as substrates to produce NTPs. Nucleoside diphosphate kinase can also form complexes with several proteins, and this has been shown to alter the specificity of substrate binding thereby directing the synthesis of specific NTPs as required during active cell growth. For example, *M. tuberculosis* cell wall protein A, a homologue of protein P_{60} in *Mycobacterium smegmatis*, can induce the specificity of nucleoside diphosphate kinase towards CTP synthesis [39]. Therefore, we propose that the broad specificity observed in this study for the *Mt*DTBS provides the tuberculi with the potential to scavenge alternative NTPs depending upon availability. This previously unrecognized mechanism ensures that the activity of this important enzyme, and the biotin biosynthetic pathway, is maintained.

ACKNOWLEDGEMENTS

This work was supported by the National Health and Medical Research Council of Australia (applications APP1011806 & APP1068885) and the Centre of Molecular Pathology, University of Adelaide. WS was a recipient of the Royal Thai Government Scholarship. MCJW is an Australian National Health and Medical Research Council of Australia Senior Research Fellow. The authors are grateful to Dr Stephan Meding, Mr James Eddes, and Mr Chris Cursaro of the Adelaide Proteomics Center at The University of Adelaide for help in mass spectrometry. We also acknowledge the computer resources of the Victorian Partnership for Advanced Computing and the Adelaide Protein Characterization Facility for access to the BIAcore. We also thank Rebecca Chao, Samuel Munday, and Kayla Downey for help in plasmid construction and preparation of the enzymes. The authors acknowledge that they have no conflict of interest to declare.

REFERENCES

[1]. Marquet, A., Tse Sum Bui, B., & Florentin, D. (2001). Biosynthesis of biotin and lipoic acid. *Vitam. Horm., 61*, 51-101.

[2]. Eisenreich, W., Dandekar, T., Heesemann, J., & Goebel, W. (2010). Carbon metabolism of intracellular bacterial pathogens and possible links to virulence. *Nat Rev Microbiol, 8*, 401-412.

[3]. Salaemae, W., Azhar, A., Booker, G., & Polyak, S. (2011). Biotin biosynthesis in *Mycobacterium tuberculosis*: physiology, biochemistry and molecular intervention. *Prot. Cell, 2*(9), 691-695.

[4]. Minnikin, D., Kremer, L., Dover, L., & Besra, G. (2002). The methyl-branched fortifications of Mycobacterium tuberculosis. *Chem Biol, 9*, 545-553.

[5]. Polyak, S., Abell, A., Wilce, M., Zhang, L., & Booker, G. (2012). Structure, function and selective inhibition of bacterial acetyl-coa carboxylase. *Appl Microbiol Biotechnol, 93*, 983-992.

[6]. Parsons, J., & Rock, C. (2011). Is bacterial fatty acid synthesis a valid target for antibacterial drug discovery? *Curr Opin Microbiol 14*, 544-549.

[7]. Chan, D., & Vogel, H. (2010). Current understanding of fatty acid biosynthesis and the acyl carrier protein. *Biochemistry, 430*, 1-19.

[8]. Keer, J., Smeulders, M. J., Gray, K. M., & Williams, H. D. (2000). Mutants of *Mycobacterium smegmatis* impaired in stationary-phase survival. *Microbiology, 146 (Pt 9)*, 2209-2217.

[9]. Rengarajan, J., Bloom, B. R., & Rubin, E. J. (2005). Genome-wide requirements for *Mycobacterium tuberculosis* adaptation and survival in macrophages. *Proc. Natl. Acad. Sci. USA, 102*(23), 8327-8332. doi: 10.1073/pnas.0503272102

[10]. Yu, J., Niu, C., Wang, D., Li, M., Teo, W., Sun, G., . . . Gao, Q. (2011). MMAR_2770, a new enzyme involved in biotin biosynthesis, is essential for the growth of Mycobacterium marinum in macrophages and zebrafish. *Microbes Infect, 13*(1), 33-41. doi: 10.1016/j.micinf.2010.08.010

[11]. Sassetti, C. M., & Rubin, E. J. (2003). Genetic requirements for mycobacterial survival during infection. *Proc. Natl. Acad. Sci. USA, 100*(22), 12989-12994. doi: 10.1073/pnas.2134250100

[12]. Park, S., Klotzsche, M., Wilson, D., Boshoff, H., Eoh, H., Manjunatha, U., . . . Schnappinger, D. (2011). Evaluating the sensitivity of *Mycobacterium tuberculosis* to biotin deprivation using regulated gene expression. *PLoS Pathogen, 7*(9), 1-10.

[13]. Feng, Y., Napier, B., Manandhar, M., Henke, S., Weiss, D., & Cronan, J. (2014). A Francisella virulence factor catalyses an essential reaction of biotin synthesis. *Mol Microbiol, 91*(2), 300-314.

[14]. Kack, H., Gibson, K., Lindqvist, Y., & Schneider, G. (1998). Snapshot of a phosphorylated substrate intermediate by kinetic crystallography. *Proc. Natl. Acad. Sci. USA, 95*, 5495-5500.

[15]. Dey, S., Lane, J., Lee, R., Rubin, E., & Sacchettini, J. (2010). Structural characterization of the Mycobacterium tuberculosis biotin biosynthesis enzymes 7,8-Diaminopelargonic acid synthase and Dethiobiotin synthetase. *Biochemistry, 49*(31), 6746-6760. doi: 10.1021/bi902097j

[16]. Yang, G., Sandalova, T., Lohman, K., Lindqvist, Y., & Rendina, A. (1997). Active site mutants of *Escherichia coli* Dethiobiotin synthetase: Effects of mutations on enzyme catalytic and structural properties. *Biochemistry, 36*, 4751-4760.

[17]. Huang, W., Jia, J., Gibson, K., Taylor, W., Rendina, A., Schneider, G., & Lindqvist, Y. (1995). Mechanism of an ATP-dependent carboxylase, Dethiobiotin synthetase, based on crystallographic studies of complexes with substrates and a reaction Intermediate. *Biochemistry, 34*(35), 10985-10995.

[18]. Porebski, P., Klimecka, M., Chruszcz, M., Nicholls, R., Murzyn, K., Cuff, M., . . . Minor, W. (2012). Structural characterization of *Helicobacter pylori* Dethiobiotin synthetase reveals differences between family members. *FEBS J, 279*, 1093-1105.

[19]. Gibson, K., Lorimer, G., Rendina, A., Taylor, K., Cohen, G., Gatenby, A., . . . Chi, H. (1995). Dethiobiotin synthetase: The carbonylation of 7,8-Diaminononanoic

acid proceeds regiospecifically via the N7-Carbamate. *Biochemistry, 34*, 10976-10984.

[20]. Wilson, D., Shi, C., Duckworth, B., Muretta, J., Manjunatha, U., Sham, Y., . . . Aldrich, C. (2011). A continuous fluorescence displacement assay for BioA: an enzyme involved in biotin biosynthesis. *Anal Biochem, 416*, 27-38.

[21]. Mann, S., Eveleigh, L., Lequin, O., & Ploux, O. (2012). A microplate fluorescence assay for DAPA aminotransferase by detection of the vicinal diamine 7,8-diaminopelargonic acid. *Anal Biochem, 432*(2), 90-96.

[22]. Sambrook, J., Fritsch, E., & Maniatis, T. (1989). *Molecular cloning: a laboratory manual* (2nd ed.). Cold Spring Harbor, N.Y.: Cold Spring Harbor Laboratory.

[23]. Ng, B., Polyak, S. W., Bird, D., Bailey, L., Wallace, J. C., & Booker, G. W. (2008). *Escherichia coli* biotin protein ligase: characterization and development of a high-throughput assay. *Anal Biochem, 376*(1), 131-136. doi: 10.1016/j.ab.2008.01.026

[24]. Lea, W. A., & Simeonov, A. (2011). Fluorescence polarization assays in small molecule screening. *Exp. Opin. Drug Discov., 6*(1), 17-32. doi: 10.1517/17460441.2011.537322

[25]. Zhang, S., Chen, L., Kumar, S., Wu, L., Lawrence, D. S., & Zhang, Z. Y. (2007). An affinity-based fluorescence polarization assay for protein tyrosine phosphatases. *Methods, 42*(3), 261-267. doi: 10.1016/j.ymeth.2007.02.008

[26]. Kabsch, W. (2010). XDS. *Acta Crystallogr D Biol Crystallogr, 66*(Pt 2), 125-132. doi: 10.1107/S0907444909047337

[27]. McCoy, A. J., Grosse-Kunstleve, R. W., Adams, P. D., Winn, M. D., Storoni, L. C., & Read, R. J. (2007). Phaser crystallographic software. *J. Appl. Crystallogr., 40*(Pt 4), 658-674. doi: 10.1107/S0021889807021206

[28]. Emsley, P., Lohkamp, B., Scott, W. G., & Cowtan, K. (2010). Features and development of COOT. *Acta Crystallogr D Biol Crystallogr, 66*(Pt 4), 486-501. doi: 10.1107/S0907444910007493

[29]. Adams, P. D., Afonine, P. V., Bunkoczi, G., Chen, V. B., Davis, I. W., Echols, N., . . . Zwart, P. H. (2010). PHENIX: a comprehensive Python-based system for macromolecular structure solution. *Acta Crystallogr D Biol Crystallogr, 66*(Pt 2), 213-221. doi: 10.1107/S0907444909052925

[30]. Checovich, W., Bolger, R., & Burke, T. (1995). Fluorescence polarization - a new tool for cell and molecular biology. *Nature, 375*, 254-256.

[31]. Niemeyer, C., Ceyhan, B., & Blohm, D. (1999). Functionalization of Covalent DNA-Streptavidin Conjugates by Means of Biotinylated Modulator Components. *Bioconjugate Chem., 10*, 708-719.

[32]. Schray, K., & Artz, P. (1988). Determination of Avidin and Biotin by Fluorescence Polarization. *Anal. Chem., 60*, 853-855.

[33]. Krell, K., & Eisenberg, M. (1970). The purification and properties of dethiobiotin synthetase. *J. Biol. Chem., 245*(24), 6558-6566.

[34]. Via, A., Ferre, F., Brannetti, B., Valencia, A., & Helmer-Citterich, M. (2000). Three-dimensional view of the surface motif associated with the P-loop structure: Cis and Trans cases of convergent evolution. *J. Mol. Biol., 303*, 455-465.

[35]. Huang, W., Lindqvist, Y., Schneider, G., Gibson, K., Flint, D., & Lorimer, G. (1994). Crystal-structure of an ATP-dependent carboxylase, dethiobiotin synthetase, at 1.65-angstrom resolution. *Structure (London), 2*, 407-414.

[36]. Buckstein, M., He, J., & Rubin, H. (2008). Characterization of nucleotide pools as a function of physiological state in Escherichia coli. *J Bacteriol, 190*(2), 718-726.

[37]. Bochner, B., & Ames, B. (1982). Complete analysis of cellular nucleotides by two dimensional thin-layer chromatography. *J. Biol. Chem., 257*, 9759-9769.

[38]. Chakrabarty, A. (1998). Nucleoside diphosphate kinase: role in bacterial growth, virulence, cell signalling and polysaccharide synthesis. *Mol Microbiol, 28*(5), 875-882.

[39]. Shankar, S., Hershberger, C., & Chakrabarty, A. (1997). The nucleoside diphosphate kinase of Mycobacterium smegmatis: identification of protiens that modulate specificity of nucleoside triphosphate synthesis by the enzyme. *Mol Microbiol, 24*(3), 477-487.

FIGURE LEGENDS

Fig. 1. NTP specificity. The specificity of *Mt*DTBS (black bars) and *Ec*DTBS (white bars) for different nucleotides was measured in the presence of 0.1 mM DAPA, 10 mM $NaHCO_3$, and 0.3 mM NTP. The specificity is presented as the percentage of enzyme activity normalized to 100% of enzyme activity using ATP.

Fig. 2. Enzyme analysis. The K_m of nucleotide substrates for both *Mt*DTBS (A – C) and *Ec*DTBS (D – F) were determined by varying the concentrations of ATP, CTP and GTP in the reaction containing 0.1 mM DAPA and 10 mM $NaHCO_3$.

Fig. 3. NTP Binding to DTBS. Competitive binding assays using a fluorescent ATP tracer and various NTPs to (A) *Mt*DTBS and (B) *Ec*DTBS. NTPs employed were ATP (green circle), CTP (blue square), GTP (black triangle), ITP (black star), TTP (black diamond), and UTP (black square).

Fig. 4. Surface plasmon resonance analysis. The sensorgrams represent the binding of ATP (green lines) and CTP (blue lines) to (A) *Mt*DTBS, (B) *Ec*DTBS and (C), *Ec*DTBS-N175A. (D) BSA was included as a negative control to demonstrate specific binding of nucleotide to DTBS. HEPES running buffer alone (red line) was also included. The experiment was performed at a single concentration of nucleotide (0.3 mM).

Fig. 5. Crystal structure of *Mt*DTBS in complex with CTP. (A) Cartoon diagram of the *Mt*DTBS dimer in complex with CTP. Subunit A is colored in gray and subunit B is colored in green. CTP is shown in pink stick representation. (B) The hydrogen bond network formed between amino acid residues of *Mt*DTBS and CTP is shown. Hydrogen bonds are indicated as dashed lines.

Fig. 6. Superimposition of *Mt*DTBS and *Ec*DTBS. The glycine at position Gly169 (grey), in *Mt*DTBS, is located at the equivalent position of Asn175 in *Ec*DTBS, as shown in blue. While two hydrogen bonds (shown as dashed lines) formed between the side chain of Asn175 in *Ec*DTBS and ATP (PDB # 1A82 [14], shown in cyan), these interactions are missing in *Mt*DTBS.

TABLE 1. Kinetic analysis of substrates.

Enzymes	Substrates	K_m (μM)	k_{cat} (s^{-1}) (x 10^{-3})
*Mt*DTBS	DAPA	30.2 ± 1.1	13.3 ± 0.7
	$NaHCO_3$	3074.3 ± 352.4	9.9 ± 0.6
	ATP	30.2 ± 1.7	11.7 ± 0.2
	CTP	25.2 ± 1.7	15.2 ± 0.3
	GTP	26.3 ± 0.5	11.1 ± 0.1
	ITP	17.7 ± 1.7	10.2 ± 1.2
	TTP	23.2 ± 1.4	11.8 ± 0.8
	UTP	26.1 ± 0.5	11.4 ± 0.8
*Ec*DTBS	DAPA	15.2 ± 1.7	49.0 ± 1.0
	$NaHCO_3$	599.8 ± 72.3	38.4 ± 3.4
	ATP	10.5 ± 0.8	38.6 ± 2.5
	CTP	1089.8 ± 156.8	28.1 ± 0.8
	GTP	1561.3 ± 299.2	29.0 ± 0.9
	ITP	> 0.3 mM	N/D
	TTP	> 0.3 mM	N/D
	UTP	> 0.3 mM	N/D
*Mt*DTBS-G169N	DAPA	15.1 ± 5.7	0.9 ± 0.3
	$NaHCO_3$	10385.3 ± 2248.0	1.7 ± 0.4
	ATP	21.5 ± 3.2	1.3 ± 0.2
	CTP	45.1 ± 4.9	1.0 ± 0.1
	GTP	100.7 ± 12.8	1.2 ± 0.1
*Ec*DTBS-N175G[b]	DAPA	18.0 ± 2.3	23.2 ± 3.2
	$NaHCO_3$	383.6 ± 64.0	15.4 ± 1.0
	ATP	17.3 ± 2.6	23.6 ± 4.6
	CTP	869.0 ± 55.9	19.6 ± 2.5
	GTP	1386.8 ± 236.5	16.3 ± 1.6
*Ec*DTBS-N175A[b]	DAPA	18.8 ± 0.2	0.9 ± 0.3
	$NaHCO_3$	433.0 ± 128.4	16.2 ± 1.9
	ATP	12.3 ± 0.9	18.1 ± 3.3
	CTP	390.9 ± 97.3	19.1 ± 1.6
	GTP	1096.9 ± 121.3	18.3 ± 2.3

N/D, Not determined. K_m and K_{cat} values were calculated from three independent experiments and reported as mean ± SEM.

TABLE 2. Nucleotide binding to *Mt*DTBS and *Ec*DTBS using DTBS ATP-binding assay

Enzymes	Substrates	IC_{50} (μM)
*Mt*DTBS	ATP	348.8 ± 15.3
	CTP	54.4 ± 4.3
	GTP	596.6 ± 51.3
	ITP	520.3 ± 60.0
	TTP	622.3 ± 19.5
	UTP	636.4 ± 18.0
*Ec*DTBS	ATP	436.9 ± 39.1
	CTP	5752.6 ± 852.5
	GTP	> 2000

IC_{50} values were calculated from three independent experiments and reported as mean ± SEM.

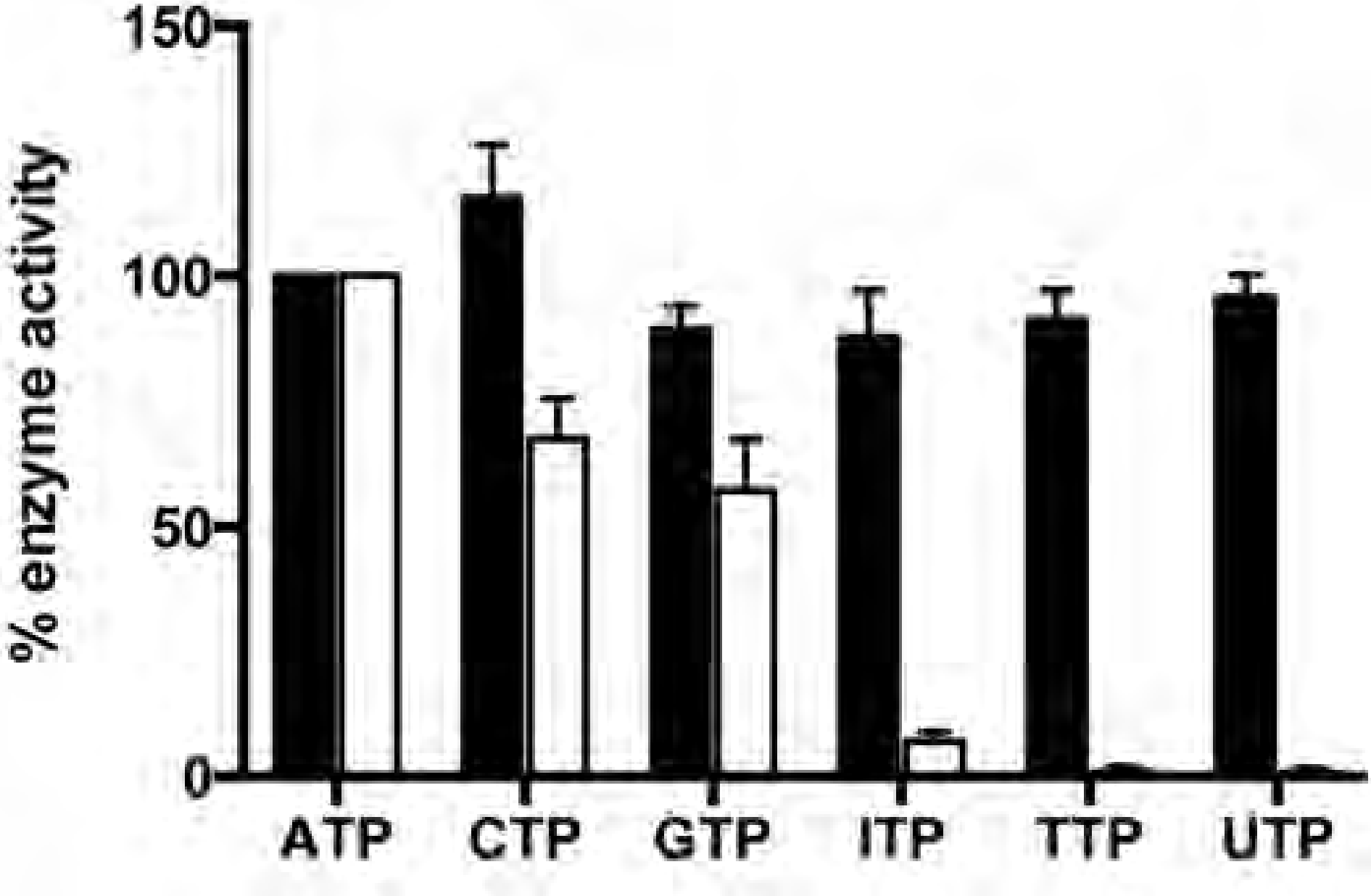
150
100
50
0
% enzyme activity
ATP
CTP
GTP
ITP
TTP
UTP

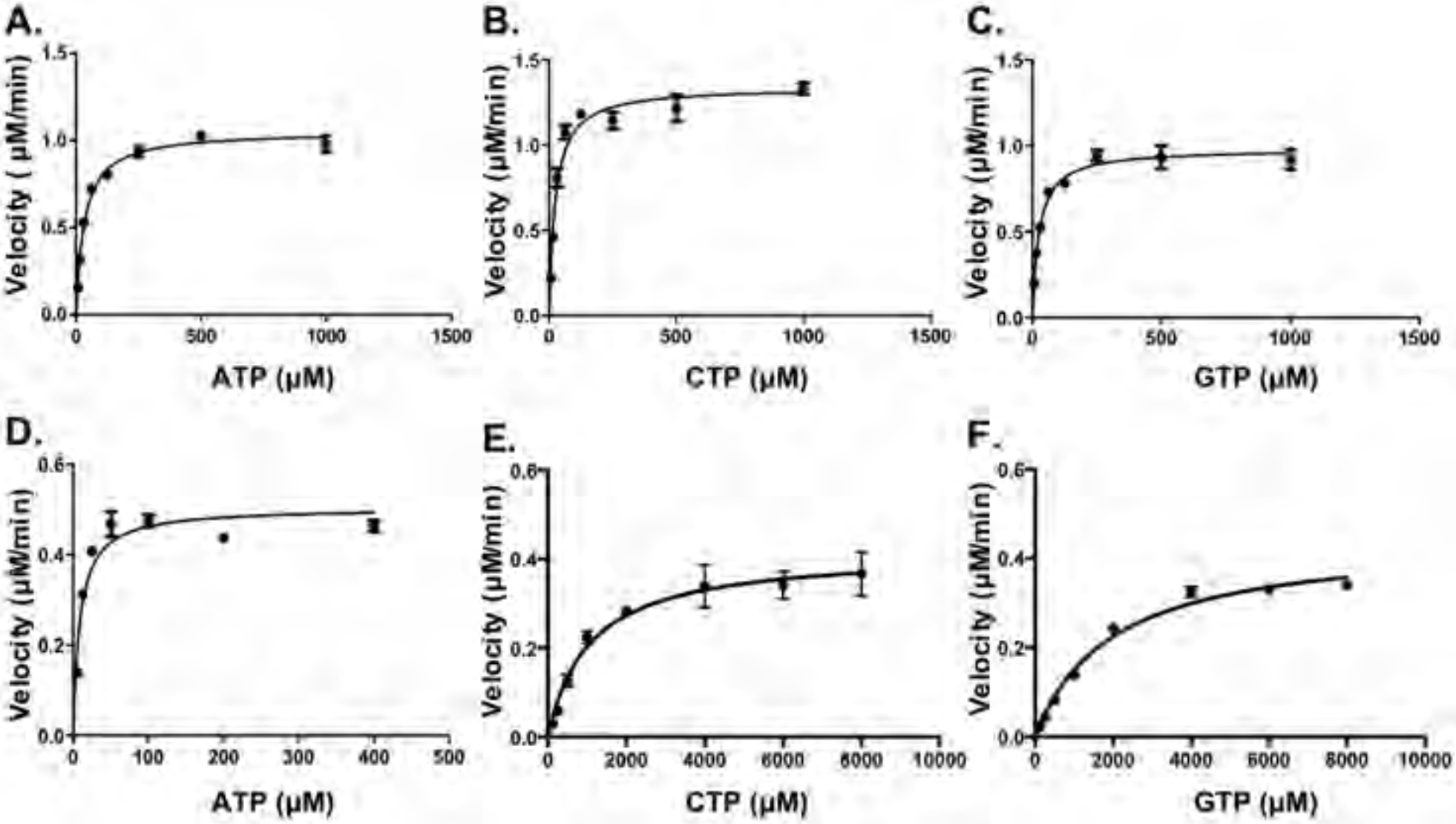
A.
Velocity (μM/min)
1.5
1.0
0.5
0.0
0
500
1000
1500
ATP (μM)
B.
Velocity (μM/min)
1.5
1.0
0.5
0.0
0
500
1000
1500
CTP (μM)
C.
Velocity (μM/min)
1.5
1.0
0.5
0.0
0
500
1000
1500
GTP (μM)
D.
Velocity (μM/min)
0.6
0.4
0.2
0.0
0
100
200
300
400
500
ATP (μM)
E.
Velocity (μM/min)
0.6
0.4
0.2
0.0
0
2000
4000
6000
8000
10000
CTP (μM)
F.
Velocity (μM/min)
0.6
0.4
0.2
0.0
0
2000
4000
6000
8000
10000
GTP (μM)

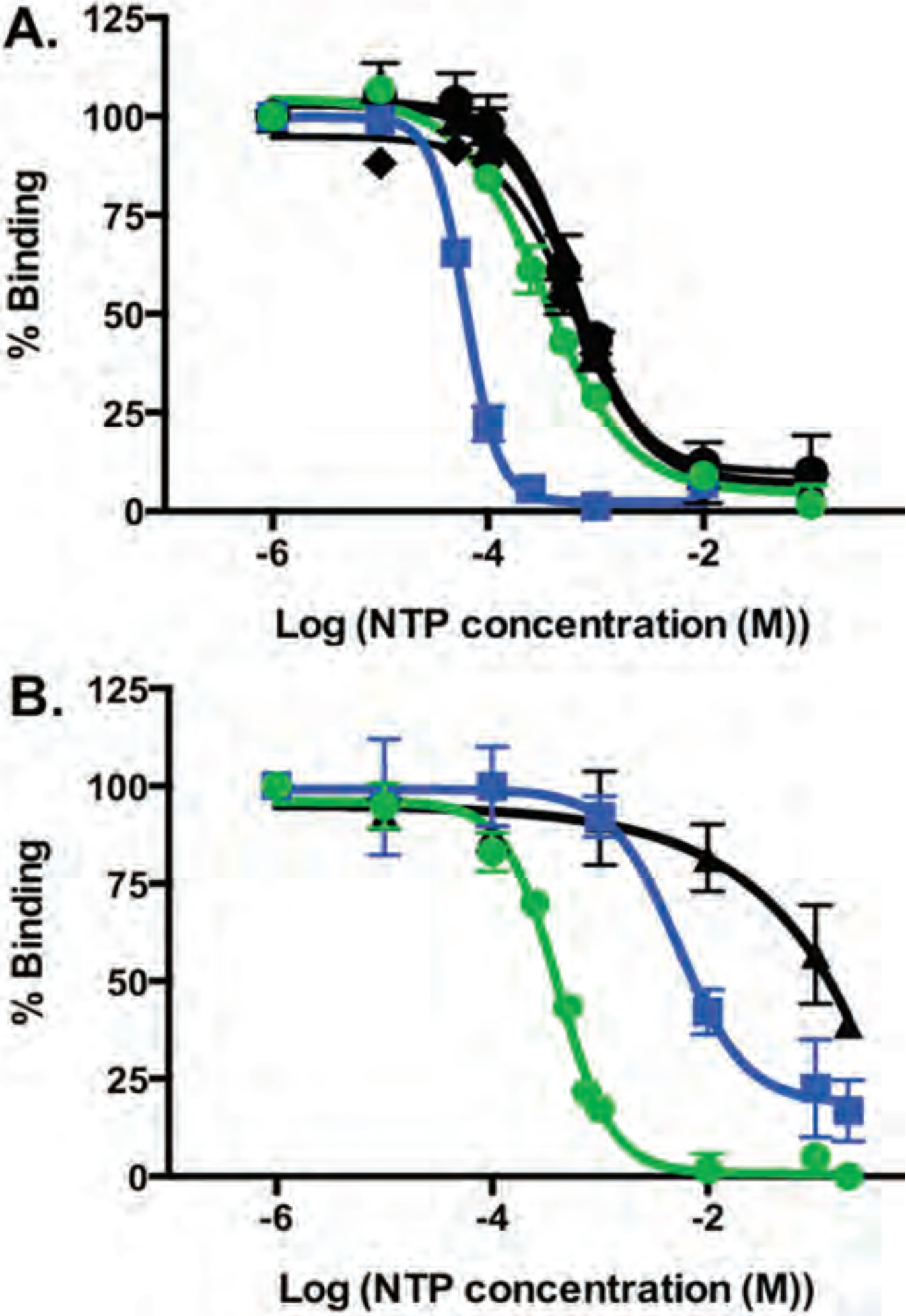
A.
125
100
75
50
25
0
% Binding
-6
-4
-2
Log (NTP concentration (M))
B.
125
100
75
50
25
0
% Binding
-6
-4
-2
Log (NTP concentration (M))

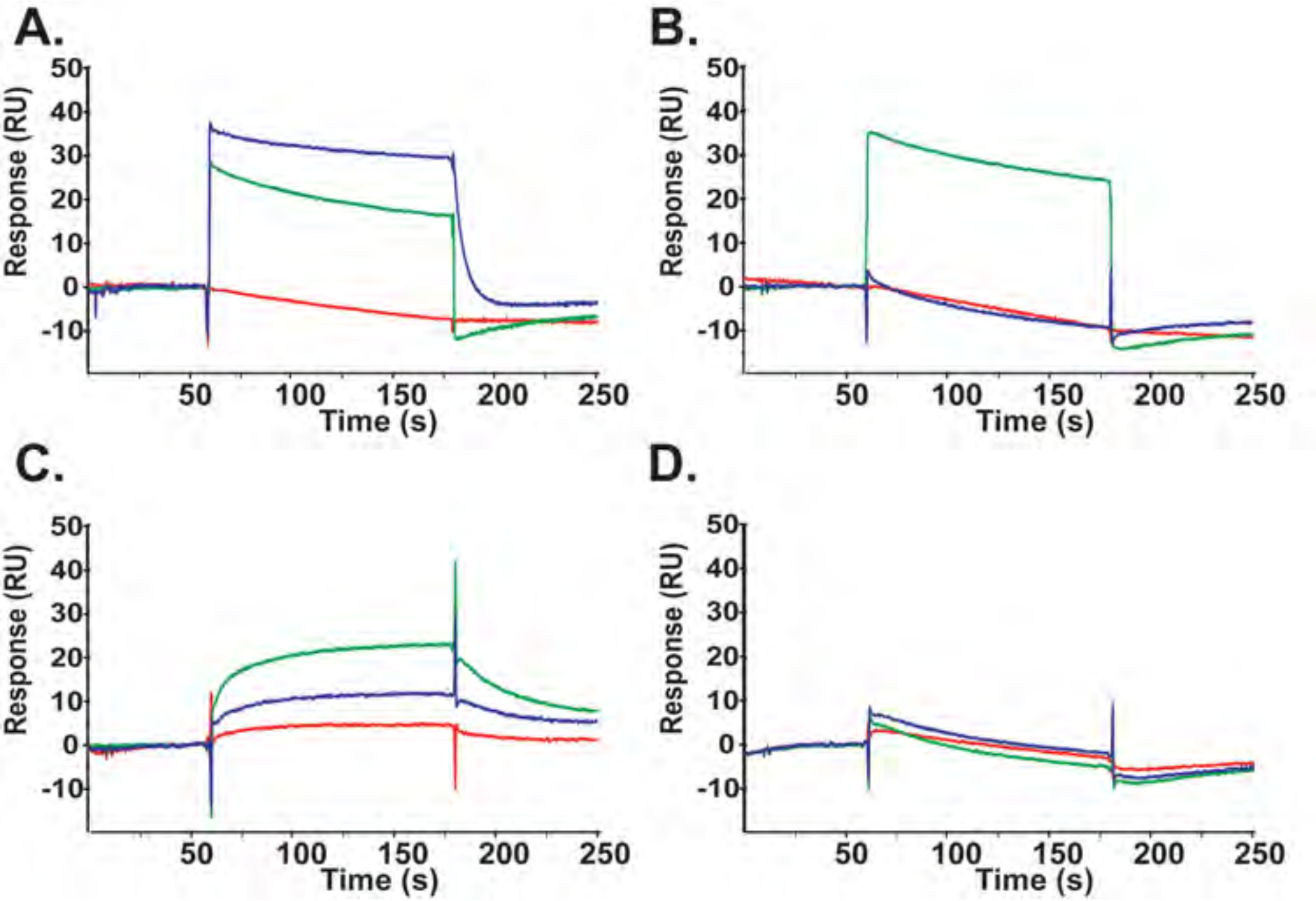
A.
B.
C.
D.
Response (RU)
Time (s)
50
40
30
20
10
0
-10
50
100
150
200
250

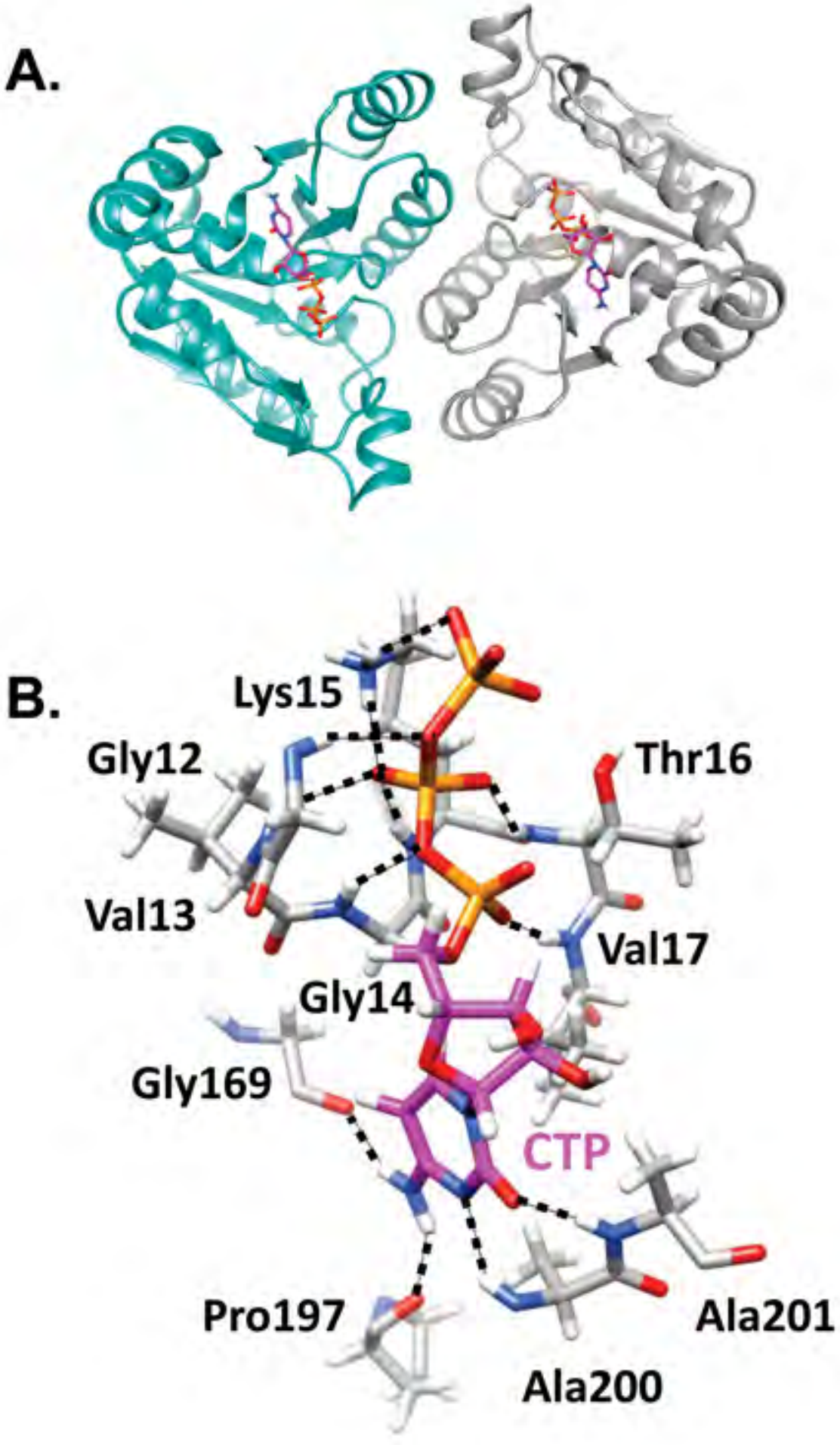
A.
B.
Lys15
Gly12
Thr16
Val13
Val17
Gly14
Gly169
CTP
Pro197
Ala201
Ala200

Nucleotide triphosphate promiscuity in *Mycobacterium tuberculosis* dethiobiotin synthetase

SUPPLEMENTARY INFORMATION

Wanisa Salaemae, Min Y. Yap , Kate L. Wegener, Grant W. Booker, Matthew C.J. Wilce and Steven W. Polyak

SUPPLEMENTARY FIGURES

Fig S1. SDS-PAGE analysis of recombinant *Mt*DTBS and *Ec*DTBS.

SDS-PAGE analysis of IMAC purified *Mt*DTBS (23.5 kDa, lane 1) and *Ec*DTBS (25.1 kDa, lane 2). The migration of molecular mass standards is shown on the left. The samples were estimated to be > 95% pure. Both proteins migrated through the gel with a size consistent with their molecular mass.

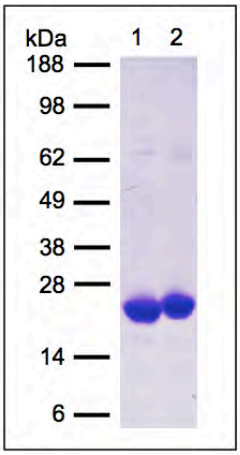

Fig S2. SEC-MALS analysis of *Mt*DTBS, *Ec*DTBS, and *Mt*DTBS-G169N.

Proteins were fractionated on a Superdex 200 10/300 GL gel filtration column connected in series with a miniDAWN TREOS light-scattering detector (Wyatt Technology) and an OPTILAB rEX interferometric refractometer detector (Wyatt Technology). Analytical size-exclusion chromatography was performed at 20° C using a mobile phase containing 25 mM Tris pH 7.5, 30 mM NaCl and 1 mM EDTA at a flow rate of 0.25 mL/min. BSA was employed as the reference sample during calibration. Chromatograms of the refractive index are shown for (A) *Mt*DTBS and (B) *Ec*DTBS. Both samples eluted with molecular masses of 47 and 46 kDa respectively, consistent with the proteins being dimers. (C) In contrast, only 25% of refolded *Mt*DTBS-G169N eluted in the dimer peak, with most of the protein observed in a high molecular mass aggregate. The percentage of the eluted protein was calculated from the proportion of the area under the curves on the chromatograms using ImageJ 1.46r (National Institute of Health, Maryland, USA).

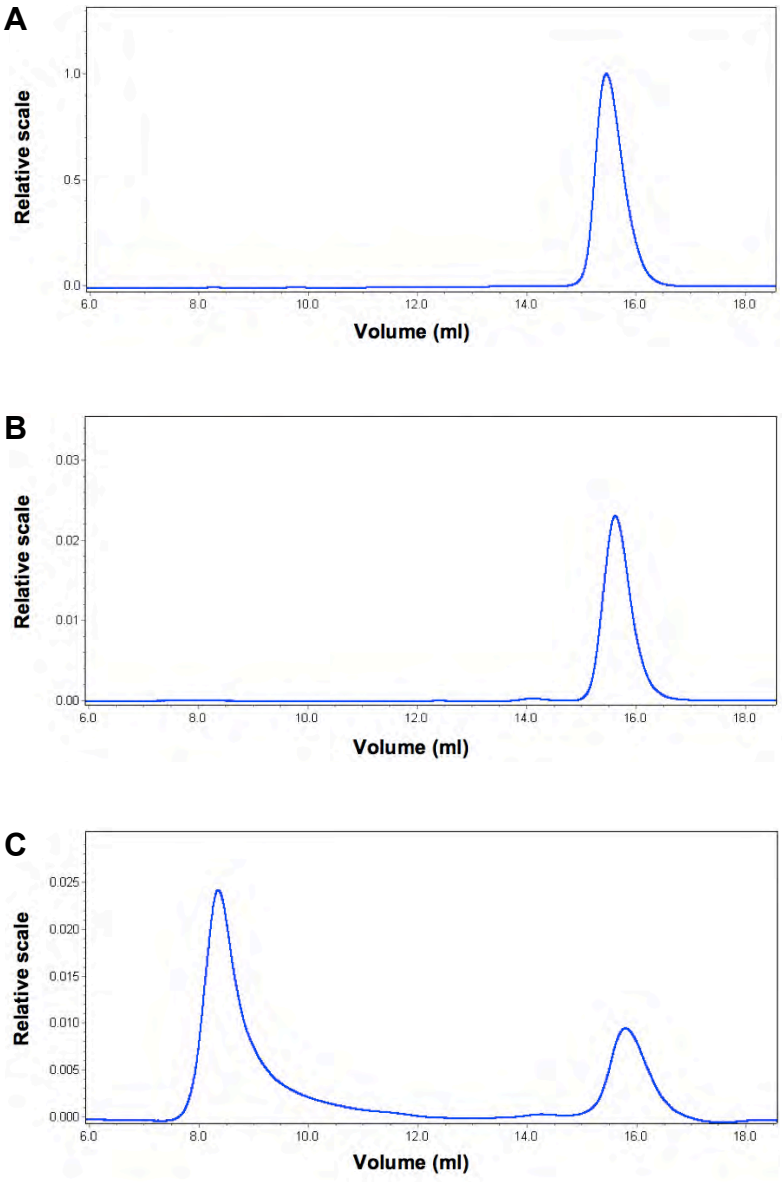

Fig S3. Controls of FP detection in DTBS enzyme assay.

A, Fluorescein-biotin does not bind to DTBS. *B*, DAPA did not displace the streptavidin:fluorescein-biotin complex in the assay containing 25 nM fluorescein-biotin and 20 nM streptavidin. Likewise, *C*, the DTBS:ATP-BODiPY complex was not disrupted by increasing concentrations of DAPA in the binding reaction implying that NTP binding is independent of DAPA. Each data point is the mean of three experiments ± SEM.

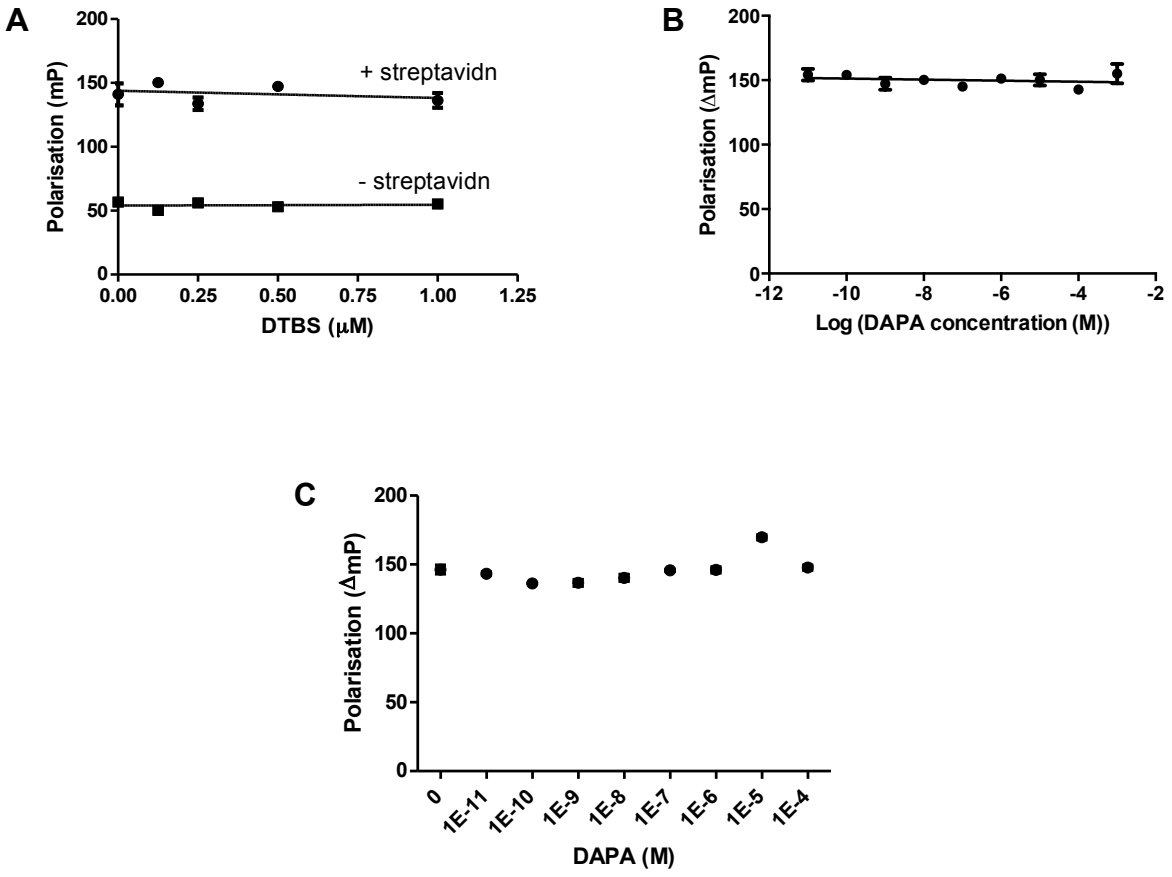

Fig S4. Surface plasmon resonance analysis.

Isotherms showing binding of (*A*) ATP and (*B*) CTP to *Mt*DTBS and (*C*) ATP to *Ec*DTBS. Data were analyzed using an affinity-steady state 1:1 model. The time-dependent binding curves of ligands correlated to dose-response are also shown (insert). The equilibrium-binding constant (K_D) of ATP and CTP to *Mt*DTBS was calculated to be 335.1 ± 96.0 μM (*n* = 3) and 17.2 ± 1.7 μM (*n* = 3). The K_D for ATP binding to *Ec*DTBS was calculated to be 347.9 ± 75.1 μM (*n* = 3). No response was observed using CTP and *Ec*DTBS (data not shown).

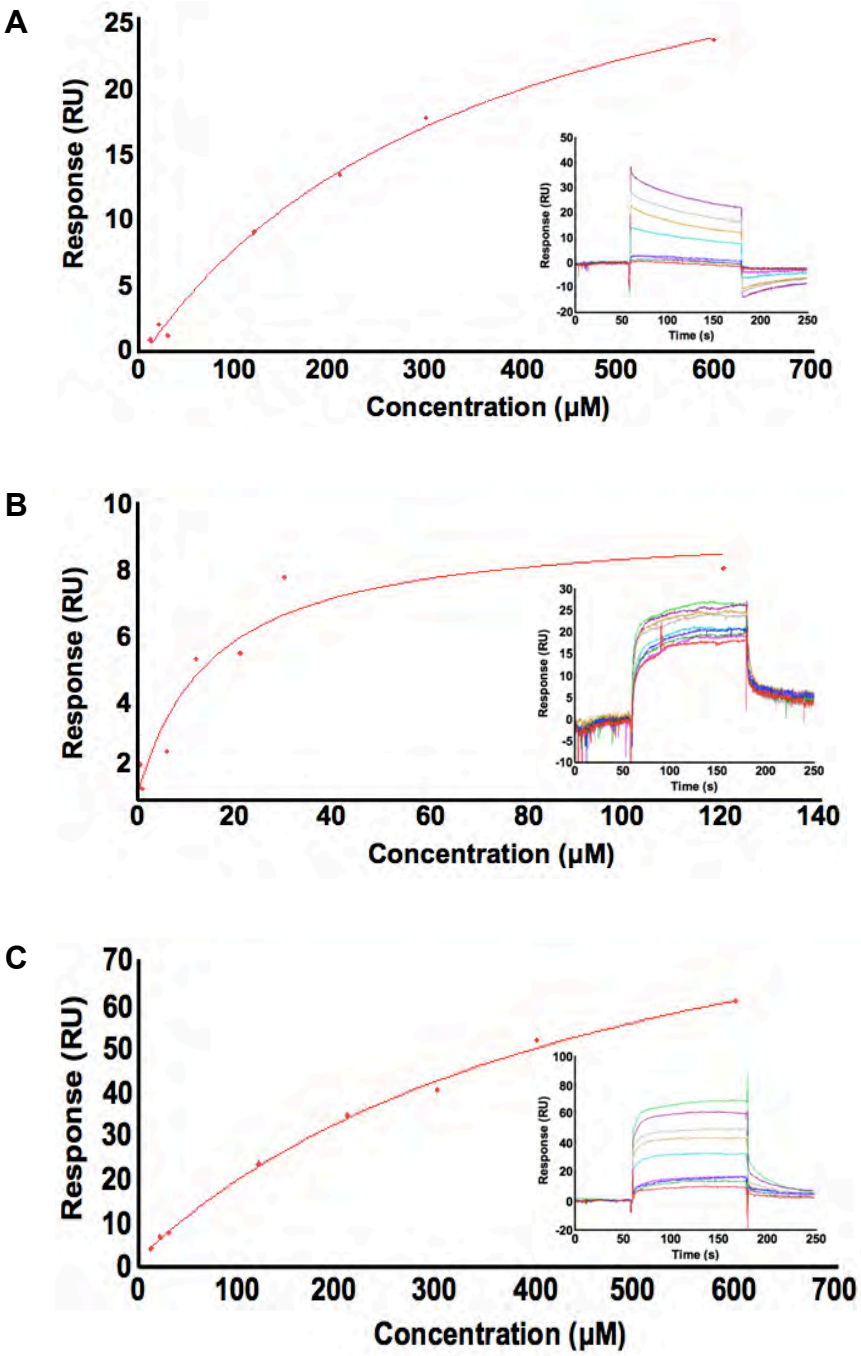

Fig S5. Mode of CTP binding within the *Mt*DTBS active site.

Residues interacting with the substrate CTP in the DTBS active site are shown in this figure, prepared using Ligplot. The protein residues are colored brown, and the ligand CTP is colored purple. Hydrogen bonds are shown in green dotted lines. Hydrophobic interactions are shown in brick red sunbursts. Atoms are colored by type (Carbon, black; Oxygen, red; Nitrogen, blue).

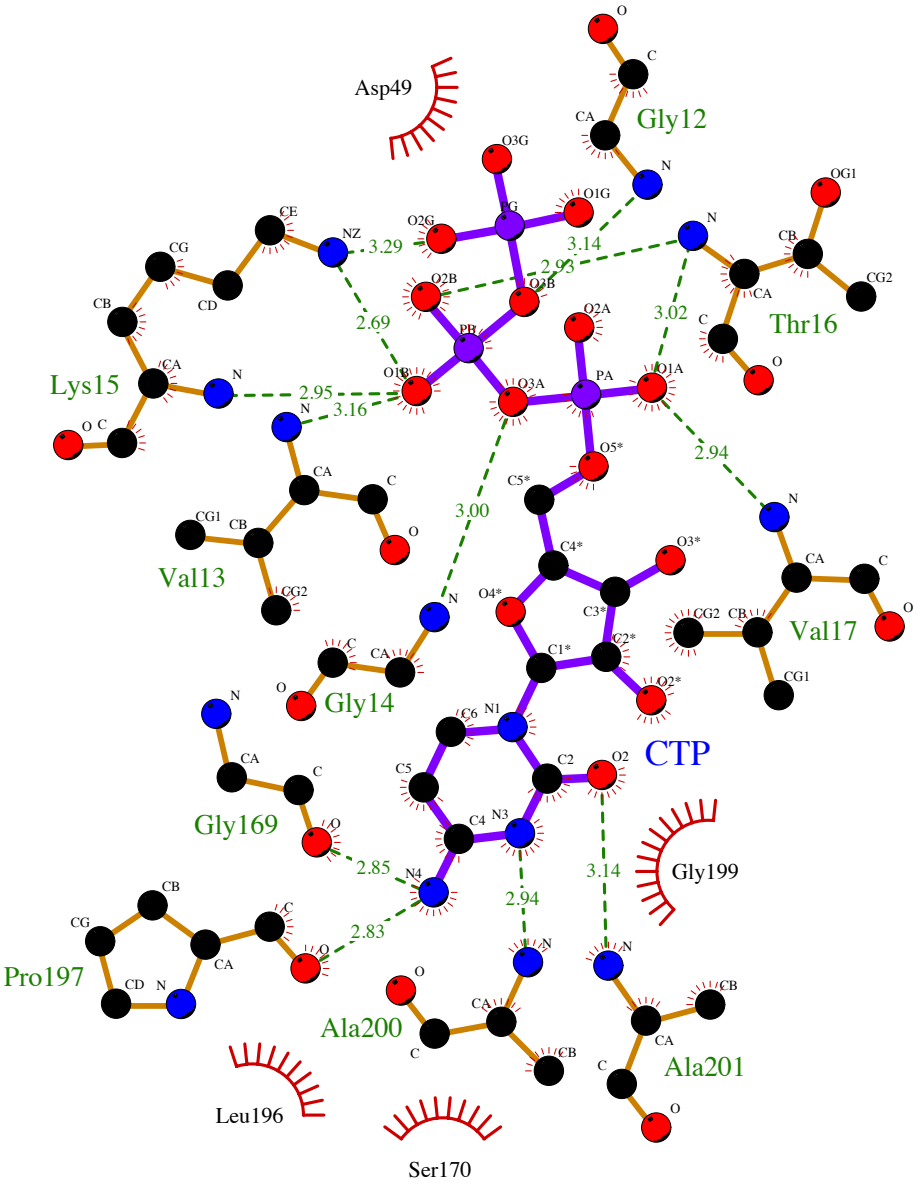

Fig S6. Representative calibration curve of DTB concentration.

The concentration of DTB was determined from a standard curve generated by incubating 25 nM fluorescein-biotin and 20 nM streptavidin with varying amounts of DTB. Each DTB concentration was assayed in triplicate, and the data points represented on the graph represent the mean ± SEM.

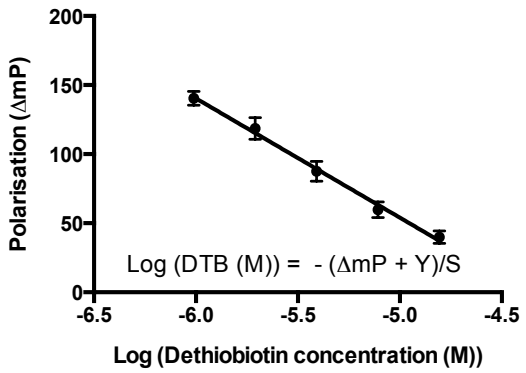

SUPPLEMENTARY TABLES

TABLE S1. Oligonucleotides employed for site-directed mutagenesis

ID	Sequence
A1	5´GCCGGTCTGGTTATTAATAGCTGGCCTGATCCGC
A2	5´GCGGATCAGGCCAGCTATTAATAACCAGACCGGC
A3	5´CTGGCGGGTTGGGTGGCGGGCGATGTTACGCCTCCGGGAAAACG
A4	5´CTGTTTCCCGGAGGCGTAACATCGCCCGCCACCCAACCCGCCAG
A5	5´CTGGCGGGTTGGGTGGCGGCCGATGTTACGCCTCCGGGAAAACG
A6	5´CGTTTTCCCGGAGGCGTAACATCGGCCGCCACCCAACCCGCCAG

TABLE S2. Mascot LC-ESI-MS/MS search results

Samples	Matched Protein	ID[a] / Total queries[b]	Sequence coverage (%)
*Mt*DTBS	His_6-*Mt*DTBS	158 / 593	47
*Ec*DTBS	ATP-dependent *Ec*DTBS (trIB1X7A8IB1X7A8_ECODH)	221 / 586	41

[a] The number of queries that were matched to a single protein, [b] The number of queries resulting from LC-ESI-MS/MS run

TABLE S3. Data Collection, Refinement, and Geometry Statistics of *Mt*DTBS in complex with CTP

	CTP-*Mt*DTBS
Data collection	
Wavelength (Å)	1.54 (Cu anode)
Space group	P $2_12_12_1$
Cell dimensions	
a, *b*, *c* (Å)	54.7, 104.6, 152.7
α, β, γ (°)	90, 90, 90
Resolution (Å)	37.8 – 2.34* (2.42-2.34)
R_{merge}	0.15(0.9)
$CC_{1/2}$*	0.99 (0.65)
$I / \sigma I$	6.5 (1.9)
Completeness (%)	99.3 (98.2)
Redundancy	5.3 (5.3)
Refinement	
Resolution (Å)	35 – 2.25
No. of reflections	79064
R_{work} / R_{free}	0.19/0.25
No. of atoms	
Protein	1565
Ligand/ion	10
Water	412
Average B Factors (Å^2)	
Protein	63.7
Solvent	68.2
Ligands	65.1
R.m.s. deviations	
Bond lengths (Å)	0.02
Bond angles (°)	1.3
Ramachandran Plot	
% most favored regions	99.3%
Allowed regions	0.7%

* High-resolution limit determined using $CC_{1/2}$ (1)

TABLE S4. Molecular mass of the wildtype and mutant DTBS measured by MALDI-MS.

DTBS enzymes	Methionine removed mass (Da)	
	Calculated mass	Measured $[M+H]^+$mass[a]
*Mt*DTBS	23318.5	23319.5
*Mt*DTBS-G169N	23375.3	23376.3
*Ec*DTBS	25003.1	249996.1
*Ec*DTBS-N175A	24960.1	24954.1
*Ec*DTBS-N175G	24946.0	24938.7

[a] The measured mass considered the initiator methionine had been post-translationally removed.

SUPPLEMENTARY EXPERIMENTAL PROCEDURES

Surface Plasmon Resonance

The kinetics of the interaction between DTBS and NTPs were analysed using a BIAcore T100. DTBS enzymes were immobilized onto the surface of a CM5 sensor chip using amide-coupling chemistry. After activating the surface with EDC and NHS, DTBS solution at concentration of 0.2 mg ml^{-1} in 0.01 M sodium acetate buffer pH 5.2 was applied at a constant flow rate of 5 µl min^{-1} for 420 s. Approximately 10,000 response units (RU) of ligands were immobilized. Typically, no immobilized ligand (empty flow cell) and immobilized bovine serum albumin (BSA) were performed alongside immobilized DTBS in order to correct for bulk refractive index changes with buffer and distinguish non-specific binding events, respectively. Water-soluble NTPs were diluted in running buffer (10 mM HEPES (pH 7.4), 150 mM NaCl and 0.005% (v/v) surfactant P20). Binding experiments were performed by injecting the analyte solutions across the sensor surface of all flow cells at a flow rate of 30 µl min^{-1} with a contact time of 60 sec followed by a dissociation time of 60 sec. The time-dependent binding curves from all four flow cells were monitored simultaneously.

As the analyte bound to the immobilized DTBS, the refractive index at the surface alters in proportion to the change in mass, resulting in change of RU value. The binding capacity of the surface depends on the level and activity of immobilized ligand. The maximum binding capacity (R_{MAX}) of the immobilized ligand was calculated using Equation 1 where MW is the molecular weight of the ligand and analyte, RL is the amount of immobilized ligand in RU, and S_M is the stoichiometry as defined by the number of binding sites on the ligand (Guiducci, 2010). The percent activity of the immobilized ligand that reflects the quality of binding was determined using Equation 2 (Guiducci, 2010).

Equation 1: $$R_{MAX} = (MW_{analyte} / MW_{ligand}) \times RL \times S_M$$

Equation 2: $$\% \text{ ligand activity} = (Rmax_{experiment} / Rmax_{theory}) \times 100\%$$

The binding affinity (K_D) was determined by transforming the time-dependent binding curves into an affinity steady-state 1:1 model using BIAcore T100 evaluation software (GE Healthcare).

Mass Spectrometry

LC-ESI-MS/MS was acquired using an 1100 series HPLC system (Agilent Technologies) coupled via an Advance CaptiveSpray source (Michrom Bioresources, Inc.) to an amaZon ETD mass spectrometer (Bruker Daltonics). Samples were initially run on a 4-12% gradient SDS-PAGE gel and stained with coomassie blue dye. Bands were excised from the gel manually and processed with a trypsin digestion protocol (Shevchenko *et al.*, 2006). Collision-induced dissociation (CID) spectra were acquired to

select the two most abundant ionisable species in the 300-2000 m/z range at any point in the LC separation. The acquired spectra were subjected to peak detection and de-convolution using DataAnalysis version 4.0 SP4 Build 281 (Bruker Daltonics). Processed MS/MS spectra were exported to Mascot generic format (mgf) and submitted to Mascot version 2.3.02 for identification by comparison to the amino acid sequences of His_6-*Mt*DTBS, His_6-*Ec*DTBS, *Mt*DTBS, *Ec*DTBS and common contaminants (i.e. human keratins and porcine trypsin) from Uniprot.

MALDI-MS was acquired on an ultrafleXtreme MALDI-TOF/TOF mass spectrometer (Bruker Daltonics) operating in a linear positive mode under the control of flexControl software version 3.4 (Bruker Daltonik GmbH). Samples were desalted by spotting onto nitrocellulose filters 0.025 µm MF-membrane filters VSWP0500 (Millipore) and dialyzing in 800 ml of 0.1% TFA for 2 hr. One microliter of each sample was mixed with 1 µl of sinapinic acid saturated TA30 (30% ACN in 0.1% FA). Next, the sample matrix was prepared by spotting the 1 µl sample mix onto the dried matrix spots which were previously spotted with 2 µl of sinapinic acid saturated ethanol onto a ground steel target plate (Bruker Daltonics) and then air dried. Sample *m/z* range was set to 5000 – 55000 Da. 50000 shots were collected for the external calibration and sample measurement. External calibration was performed using a mix of protein calibration standard I and II (Bruker Daltonics). Laser intensity and detector gain was manually adjusted for optimal resolution. The MS spectra obtained were analysed using flexAnalysis software version 3.3 (Bruker Daltonics) employing smoothing, background subtraction and peak detection algorithms.

SUPPLEMENTARY REFERENCES

Guiducci, C., (2010) Advanced bioengineering methods laboratory: SPR. In: Ecole Polytechnique Federale De Laussanne. pp.

Shevchenko, A., H. Tomas, J. Havlis, J. Olsen & M. Mann, (2006) In-gel digestion for mass spectrometric characterization of proteins and proteomes. *Nat. Protoc.* **1**: 2856-2860.